

Chiral Meissner effect in time-reversal invariant Weyl superconductors

Vira Shyta,¹ Jeroen van den Brink,^{1,2} and Flavio S. Nogueira¹

¹*Institute for Theoretical Solid State Physics, IFW Dresden, Helmholtzstr. 20, 01069 Dresden, Germany*

²*Institute for Theoretical Physics and Würzburg-Dresden Cluster of Excellence ct.qmat, TU Dresden, 01069 Dresden, Germany*

Weyl semimetals are characterised by pairs of topologically protected nodes at which electronic bands cross and electrons attain a definite chirality. Due to the chiral anomaly, the non-conservation of charges with given chirality, the axion term appears in their effective electromagnetic action. We determine how this affects the properties of time-reversal invariant Weyl *superconductors* (SCs) in the London regime. For type II SCs we show that axion coupling generates magnetic B -fields transverse to a vortex. Above a critical axion coupling vortices become unstable and a transition into a type I SC follows. In this regime an applied B -field not only decays inside the SC within the London penetration depth, but the axion coupling generates an additional perpendicular field. Consequently the B -field inside the superconductor progressively rotates away from the applied one when going into the bulk. At a critical coupling the Meissner state breaks down. The novel chiral SC state that then emerges has a periodically divergent susceptibility, at which the winding of B inside the superconductor jumps. Thus the axion coupling leaves crisp experimentally observable signatures in Weyl SCs.

Introduction— Experimentally superconductivity has been reported in a number of Weyl semimetals, both at ambient [1–6] and high pressures [7, 8]. The topological nature of Weyl semimetals [9–15] gives hope that Majorana zero modes bounded to vortices [16, 17] may be detected in the future. Another recent experimental development in the field was the recently found superconductivity in the time-reversal invariant (TRI) Weyl semimetal PtBi₂ [5, 6, 18], where the superconducting state seems to occur only on the surface of the material. Accordingly, a Berezinskii-Kosterlitz-Thouless phase transition [19, 20] was reported to occur [5].

As the low-energy electromagnetic response of superconductors (SCs) is governed by the London equations, the question arises how the presence of Weyl nodes modifies the electromagnetic properties of these Weyl superconductors, in particular as to their Meissner effect for a type I and magnetic vortices for a type II SC. Here we consider the London electrodynamics of TRI Weyl superconductors [9–15], which in the case of Weyl semimetals originates from the axion action,

$$S_a = \frac{\alpha}{4\pi^2} \int dt \int d^3r \vartheta(t, \mathbf{r}) \mathbf{E} \cdot \mathbf{B}, \quad (1)$$

where α is the fine-structure constant and the axion field is assumed to have the explicit form $\vartheta(t, \mathbf{r}) = \mathbf{b} \cdot \mathbf{r} - b_0 t$. Here \mathbf{b} and b_0 represent the separation between Weyl nodes in momentum and energy, respectively [14, 15]. Specifically, we will be interested here in the case where TRI holds, which leads to a net $\mathbf{b} = 0$ due to the presence of time reversed Weyl node pairs. A typical physical consequence of the axion response is the chiral magnetic effect (CME) [21–23], which implies that the current density contains a contribution $\mathbf{j}_{\text{CME}} = -a\mathbf{B}/(4\pi)$, where a is the axion coupling constant, related to b_0 . Here we uncover a number of novel electrodynamic features that follow from the interplay between the axion-induced CME and superconductivity in Weyl systems.

Within the London theory the superconducting current is given by $\mathbf{j}_{\text{SC}} = q\rho_s(\nabla\theta - q\mathbf{A})$, where ρ_s is the superfluid stiffness, $q = 2e$ is the charge, θ is the phase of the order parameter and \mathbf{A} the vector potential. Therefore, in a Weyl superconductor with TRI the total current density is given by $\mathbf{j} = \mathbf{j}_{\text{SC}} + \mathbf{j}_{\text{CME}}$.

As we will see, while the magnetic field expulsion from a superconductor is ensured by its current being proportional to \mathbf{A} , the contribution from CME, which is linear in \mathbf{B} , leads to a rotation in the magnetic field screening. The chiral behavior of the Meissner effect may be understood by first considering the non-superconducting phase. In this case $\nabla \times \mathbf{B} = -a\mathbf{B}$ and we see that $\nabla^2 \mathbf{B} + a^2 \mathbf{B} = 0$, which yields spatially rotating magnetic field profiles. When the system becomes superconducting, the Meissner screening twists as a response to the rotation induced by the CME.

We also find that at a critical axion coupling a_c the Meissner state breaks down and the magnetic field starts to rotate periodically inside the entire SC. The number of windings of the field inside the SC is quantized and transitions between plateaus associated with a divergence in magnetic susceptibility. Apart from this we establish how the axion coupling manifests in the vortex properties of type II Weyl SCs. Since the vortex appears as a response to the external magnetic field, the magnetic field inside of the vortex is expected to be directed along the vortex line. However, in a Weyl superconductor another, transverse component of the magnetic field is induced. Due to the competition between the axion term and superconductivity a transition occurs from this chiral vortex state to a conventional one without vortices at a critical coupling a_c .

Axion London electrodynamics — Accounting for the chiral anomaly in Weyl systems, the following Lagrangian governs the electromagnetic properties of TRI Weyl su-

perconductors in the London regime

$$\begin{aligned} \mathcal{L} = & \frac{\epsilon}{8\pi} \mathbf{E}^2 - \frac{1}{8\pi} \mathbf{B}^2 + \frac{\rho_s}{2} \left[(\partial_t \theta - q\phi)^2 - (\nabla \theta - q\mathbf{A})^2 \right] \\ & - \frac{q^2}{8\pi^2} b_0 \epsilon_{0ijk} A_i \partial_j A_k, \end{aligned} \quad (2)$$

with units such that $\hbar = c = 1$. The most important equation for us following from the above Lagrangian is,

$$\nabla \times \mathbf{B} = 4\pi \mathbf{j}_{\text{SC}} + \epsilon \partial_t \mathbf{E} - a \mathbf{B}, \quad (3)$$

where $a = q^2 b_0 / \pi$. In the static regime that we consider here Eq. (3) becomes a generalized London equation having the current density of the form mentioned above, namely, one where the total current includes the CME contribution, $\mathbf{j}_{\text{CME}} = -a \mathbf{B} / (4\pi)$.

Vortex in type II Weyl SC — We first consider the fate of a magnetic vortex in presence of an axion coupling. Due to the CME current, the analysis here differs significantly from previous discussions on the subject based on the Witten effect [24], where the field of the vortex induces a fractional charge at the interface between an SC and a topological insulator [25], as well as a fractional angular momentum [26, 27]. The vortex axion physics discussed below does not involve the electric field and is intrinsic to TRI Weyl superconductors, so proximity to a topological material needs not to be assumed. Taking the curl of Eq. (3) we obtain in the static regime,

$$-\nabla^2 \mathbf{B} + a \nabla \times \mathbf{B} + M^2 \mathbf{B} = \frac{M^2 \Phi_0}{2\pi} \boldsymbol{\Omega}, \quad (4)$$

where $M^2 = 4\pi q^2 \rho_s$ represents the inverse square of the London penetration depth λ (in London theory without axion coupling $\lambda = 1/M$), $\Phi_0 = 2\pi/q$ is the elementary flux quantum, and $\boldsymbol{\Omega} = \nabla \times \nabla \theta$ is the vorticity (recall that the curl of a gradient vanishes everywhere, except there where topological defects like vortices exist [28]).

For an infinite system the exact solution is obtained by performing a Fourier transform, which leads to

$$B_i(p) = \frac{2\pi M^2 \Phi_0 \delta(p_z) \bar{p}^2}{\bar{p}^4 - a^2 p^2} \left(\delta_{iz} + \frac{ia}{\bar{p}^2} \epsilon_{izk} p_k \right), \quad (5)$$

where $\bar{p}^2 = p^2 + M^2$ and yields in real space $\mathbf{B}(\mathbf{r}) = B_\varphi(r) \hat{\boldsymbol{\varphi}} + B_z(r) \hat{\mathbf{z}}$, with

$$B_\varphi(r) = \frac{M^2 \Phi_0}{2\pi \sqrt{a^2 - a_c^2}} \sum_{\sigma=\pm} \sigma M_\sigma K_1(M_\sigma r), \quad (6)$$

$$B_z(r) = \frac{M^2 \Phi_0}{2\pi \sqrt{a^2 - a_c^2}} \sum_{\sigma=\pm} M_\sigma K_0(M_\sigma r), \quad (7)$$

where $K_\alpha(x)$ are modified Bessel functions of the second kind, and $2M_\pm = \sqrt{a_c^2 - a^2} \pm ia$, where $a_c = 2M$. Equations (6) and (7) reduce to the well known London solution when $a = 0$, yielding a magnetic field parallel to the

z -axis. The axion contribution generates a φ -component of the magnetic field and, as a consequence, a component of the current parallel to the vortex is generated. The total current screening the vortex is thus encircling it in a helical manner, with a handedness determined by the sign of a . This solution is well defined for $a < a_c$.

In Fig. 1 the magnetic induction components corresponding to the vortex solution of Eqs. (6) and (7) are displayed for different values of a . We note the fields start to develop more spatial structure with increasing a , so the Meissner effect around the vortex is not complete, with a spatially damped oscillatory behavior emerging. For values of a close to the critical value a_c the oscillations become much stronger, as shown in panels (c) and (d) of Fig. 1. For $a \geq a_c$ the argument of the Bessel functions appearing in Eqs. (6) and (7) become purely imaginary and the vortex solution breaks down. As a result, the system must transition into a type I regime. As at the SC phase transition the penetration depth λ diverges and thus M tends to zero, for any finite (and possibly small) a , the regime $a \geq a_c$ is always realized close to the SC phase transition.

The vortex solution can also be obtained exactly in a finite slab of thickness L , with the vortex line perpendicular to the surface, as discussed in the Supplemental Material. In this case it is interesting to consider the external magnetic field explicitly for the case when the vortex solution does not exist, where $a \geq a_c$. Here we can see better the perfect diamagnetic character of the phase. Actually, since for this geometry the magnetic field is perpendicular to the surface, continuity of the normal component implies that the CME current vanishes, in which case the usual London equation follows. The only possible solution henceforth is one of a vanishing magnetic induction.

Meissner effect in type I Weyl SC — Compared to the situation of an external magnetic field is applied along the surface normal of a type I London SC, where perfect diamagnetism is unaltered by the CME, the more interesting case is the one with the field applied parallel to the surface, rendering a finite London penetration depth. Here, due to the CME, we find a crucial difference relative the usual London electrodynamics: the Meissner screening works differently, since application of an external magnetic field generates additional components for the magnetic induction, as the differential equations for the field components are coupled via the axion term. As a first example, let us consider a semi-infinite superconductor located in the region $x > 0$ in the presence of an applied magnetic field $\mathbf{B}_{\text{ap}} = B_{\text{ap}} \hat{\mathbf{y}}$. For this simple geometry one obtains the coupled equations

$$-\partial_x^2 B_y + M^2 B_y - a \partial_x B_z = 0, \quad (8)$$

$$-\partial_x^2 B_z + M^2 B_z + a \partial_x B_y = 0 \quad (9)$$

with the boundary conditions, $B_y(x=0) = B_{\text{ap}}$, $B_y(x \rightarrow \infty) = 0$, $B_z(x=0) = 0$, $B_z(x \rightarrow \infty) = 0$. As with the

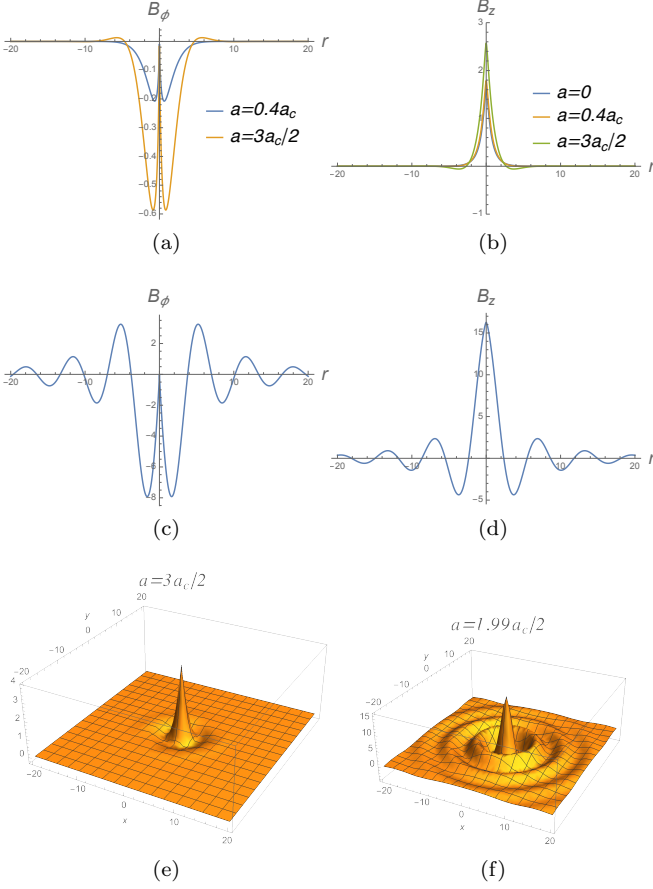


FIG. 1. Magnetic induction profiles for different values of the axion coupling a [panels (a) and (b) for the field components B_ϕ and B_z , respectively]. Fields are plotted in units of $M^2\Phi_0/(2\pi)$ against the radial coordinate r in units of M . Panels (c) and (d) show the field components for $a = 1.99a_c/2$, corresponding to a situation where a is very close to the critical value $a_c = 2M$ for which the vortex solution ceases to exist. We note that as a approaches a_c the field profiles start to become more oscillatory. The onset of these spatial oscillations is illustrated by the three-dimensional plots for B_z in panels (e) and (f) for $a = 3a_c/2$ and $a = 1.99a_c/2$, respectively.

vortex solution, there are two distinct regimes to consider: $a < a_c$ and $a > a_c$. The former yields the solution $\mathbf{B}(x) = B_{ap}e^{-(x/2)\sqrt{a_c^2 - a^2}}\hat{\mathbf{u}}(x)$ in terms of the unit vector,

$$\hat{\mathbf{u}}(x) = \cos(ax/2)\hat{\mathbf{y}} + \sin(ax/2)\hat{\mathbf{z}}, \quad (10)$$

and one observes that the field inside the SC rotates with respect to the applied one, a chiral oscillatory feature as was found for the vortex. Thus, applying a magnetic field in the y -direction does not only lead to a Meissner effect with an exponentially decaying y -component of the field, but also generates a similarly decaying field along the z -direction as a consequence of the axion coupling. The corresponding field profiles are shown in panels (a) and

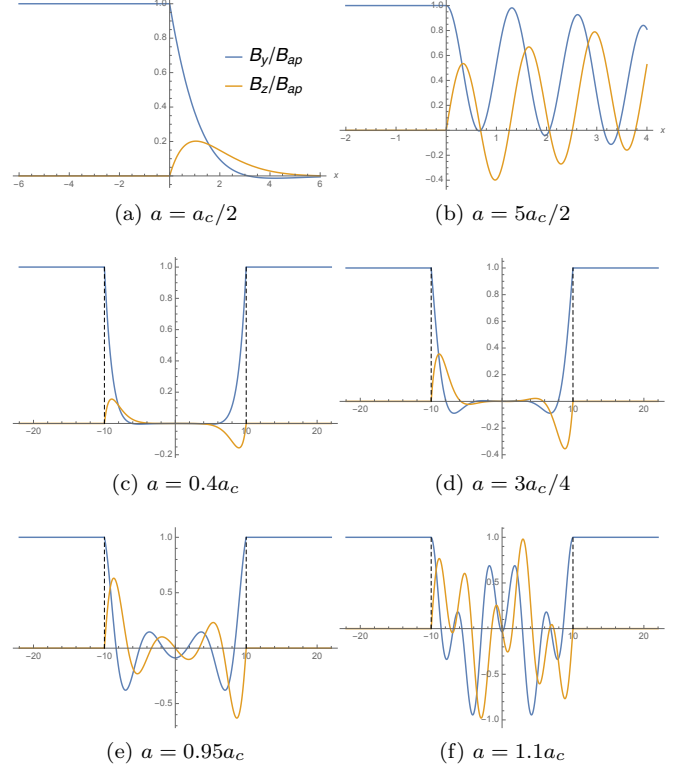


FIG. 2. Panel (a): Magnetic field components of a semi-infinite superconductor located at $x > 0$ and in the presence of an applied magnetic field, $\mathbf{B}_{ap} = B_{ap}\hat{\mathbf{y}}$. Panel (b): Absence of Meissner effect for $a = 5a_c/2$ in a semi-infinite TRI Weyl superconductor. From panels (c-e) we have $a < a_c$, corresponding to $a = 0.4a_c$, $a = 3a_c/4$, and $a = 0.95a_c$, respectively. We can see once more the onset of spatial oscillations in the magnetic induction as a increases. In panel (f) $a = 1.1a_c$, which is a little bit above its critical value. In this case the axion coupling completely dominates over Meissner screening.

(b) of Fig. 2 for exemplary values of a below and above a_c . Note that the effective penetration depth renormalized by a is given by $\lambda = 1/\sqrt{M^2 - a^2/4}$ and is larger than the unrenormalized London penetration depth $1/M$. Clearly also this effective penetration depth diverges for $a = a_c$, showing that indeed this value of a corresponds to a critical point.

For $a \geq a_c$ there is no solution that fulfils the boundary condition $B_z(x \rightarrow \infty) = 0$. Thus, instead of demanding $B_y(x \rightarrow \infty) = 0$ and $B_z(x \rightarrow \infty) = 0$, we only enforce the boundary conditions at the surface $B_y(x = 0) = B_{ap}$, $B_z(x = 0) = 0$, and require the solutions to be real, which yields

$$\mathbf{B}(x) = B_{ap} \cos(\sqrt{a_c^2 - a^2} x/2) \hat{\mathbf{u}}(x) \quad (11)$$

Remarkably, the magnetic field inside of the sample exhibits a purely oscillatory behavior and as illustrated in Fig. 2-(b) for $a = 5a_c/2$, there is no Meissner effect in

the sense that the magnetic field is eventually screened inside the bulk of the SC. Instead, it rotates around the surface normal modulated by the field magnitude as it penetrates all the way into the bulk. This brings to the fore once more the important role of the critical value $a_c = 2M$ of the axion coupling a in modifying the nature of the Meissner effect. To investigate how it precisely signals a phase transition we compute the magnetic susceptibility as a response to the applied field. This requires us to determine the average the magnetic induction over the system, which cannot be done easily in a convergent manner in semi-infinite system and it is more convenient to consider a finite slab geometry with two surfaces such that $|x| < L/2 = \bar{L}$. We obtain,

$$\mathbf{B}(x) = \frac{B_{ap}}{\sin(\bar{L}\sqrt{a^2 - a_c^2})} \times \sum_{\sigma=\pm} \sigma \sin \left[\frac{\sqrt{a^2 - a_c^2}}{2} (x + \sigma \bar{L}) \right] \hat{\mathbf{u}}(x - \sigma \bar{L}), \quad (12)$$

which has the advantage to hold any value of a . Figure 2 shows the magnetic induction profiles corresponding to Eq. (12) for increasing values of a up to slightly above a_c . The axion coupling causes a spatial rotation in the Meissner screening, causing it to disappear for $a > a_c$ when the oscillations are stronger. Remarkably, for a significantly larger than a_c the oscillation amplitude can get larger than the applied field.

In order to elucidate the behavior for $a > a_c$, we calculate the diamagnetic susceptibility χ from the spatial average of the magnetic induction. From the expressions it is clear that axion-induced field component B_z averages to zero for any a . For the component parallel to the applied field we obtain the diamagnetic susceptibility

$$\chi = \frac{\sqrt{a^2 - a_c^2}}{LM^2 \sin(\bar{L}\sqrt{a^2 - a_c^2})} \left[\cos(\bar{L}\sqrt{a^2 - a_c^2}) - \cos(a\bar{L}) \right]$$

which for $a \rightarrow a_c$ goes to $\frac{2}{M^2 L^2} [1 - \cos(ML)]$. For $ML \gg 1$, corresponding to a large slab thickness compared to the London penetration depth, χ vanishes for all $a \leq a_c$. For $a > a_c$, on the other hand, the susceptibility diverges for

$$a^2 = a_c^2 + \left(\frac{2\pi n}{L} \right)^2 \quad \text{with} \quad n \in \mathbb{N}. \quad (13)$$

Thus, at quantized values of the axion coupling the system becomes unstable. At these values the winding of the field inside the SC changes by unity. It is interesting to note that this leads to a situation reminiscent of the Little-Parks effect [29] in superconducting cylinders subjected to a parallel magnetic field, where the persistent current suppresses the cylinder's superconductivity. Although in our case no such geometry is involved, the currents generated by the CME affect the SC state of

the slab, and particularly so when the length scale associated to the axion coupling is comparable to the London penetration depth.

Conclusions and outlook — As the axion term affects the properties of Weyl superconductors in a rather non-trivial manner, several distinct experimentally testable predictions follow from our results. This is clear for the currents parallel to magnetic vortices and the magnetic fields perpendicular to them induced by the axion coupling. In future work it will be interesting to establish how this affects the vortex lattice and its stability. The vortex becoming unstable at the critical axion coupling implies a transition from a type II to a type I superconducting state. Such a transition between type I and II SC in the same material is known as type 1.5 superconductivity for multiband systems [30, 31]. As close to the SC phase transition the London penetration depth diverges the critical axion coupling vanishes there. Thus for any given axion coupling intrinsic to the Weyl SC material, close enough to the SC transition the system automatically enters the strong coupling regime where the vortex state becomes unstable and a type 1.5 regime may ensue.

In type I superconductors the axion induced magnetic field component perpendicular to the applied field and parallel to the surface may be explored by surface sensitive probes, e.g. the magneto-optic Kerr effect. It is interesting to note that the rotating B -field inside the SC also causes vortices close to the surface to cant with respect to the applied field, which results in magnetic stray fields outside the SC [32]. This is a rather intricate consequence of the emergent field components transverse to the flux line, as simple addition of a mirror vortex cannot fulfil the boundary conditions on the surface.

For strong coupling the axion renormalization of the London penetration depth may be probed experimentally, whereas the breaking down of the Meissner state is associated with a periodically divergent susceptibility, at which the winding of \mathbf{B} inside the superconductor jumps, allowing in principle for rather direct observation.

We thank Volodymyr Kravchuk for stimulating discussions. We acknowledge financial support by the Deutsche Forschungsgemeinschaft (DFG, German Research Foundation), through SFB 1143 project A5 and the Würzburg-Dresden Cluster of Excellence on Complexity and Topology in Quantum Matter-ct.qmat (EXC 2147, Project Id No. 390858490).

While preparing this manuscript we became aware of the work of M. Stålhammar et al. [33], who report semi-infinite slab and cylinder solutions similar to our results.

-
- [1] N. P. Butch, P. Syers, K. Kirshenbaum, A. P. Hope, and J. Paglione, "Superconductivity in the topological semimetal yptbi," *Phys. Rev. B* **84**, 220504 (2011).

- [2] Y. Qi, P. G. Naumov, M. N. Ali, C. R. Rajamathi, W. Schnelle, O. Barkalov, M. Hanfland, S.-C. Wu, C. Shekhar, Y. Sun, V. Süß, M. Schmidt, U. Schwarz, E. Pippel, P. Werner, R. Hillebrand, T. Förster, E. Kampert, S. Parkin, R. J. Cava, C. Felser, B. Yan, and S. A. Medvedev, “Superconductivity in weyl semimetal candidate mote2,” *Nature Communications* **7**, 11038 (2016).
- [3] H.-J. Noh, J. Jeong, E.-J. Cho, K. Kim, B. I. Min, and B.-G. Park, “Experimental realization of type-ii dirac fermions in a pdte_2 superconductor,” *Phys. Rev. Lett.* **119**, 016401 (2017).
- [4] H. Leng, C. Paulsen, Y. K. Huang, and A. de Visser, “Type-i superconductivity in the dirac semimetal pdte_2 ,” *Phys. Rev. B* **96**, 220506 (2017).
- [5] A. Veyrat, V. Labracherie, D. L. Bashlakov, F. Caglieris, J. I. Facio, G. Shipunov, T. Charvin, R. Acharya, Y. Naidyuk, R. Giraud, J. van den Brink, B. Büchner, C. Hess, S. Aswartham, and J. Dufouleur, “Berezinskii-kosterlitz-thouless transition in the type-i weyl semimetal ptbi_2 ,” *Nano Letters* **23**, 1229 (2023).
- [6] A. Kuibarov, O. Suvorov, R. Vocaturo, A. Fedorov, R. Lou, L. Merkwitz, V. Voroshnin, J. I. Facio, K. Koepnik, A. Yaresko, G. Shipunov, S. Aswartham, J. van den Brink, B. Büchner, and S. Borisenko, “Superconducting arcs,” (2023), [arXiv:2305.02900 \[cond-mat.supr-con\]](https://arxiv.org/abs/2305.02900).
- [7] D. Kang, Y. Zhou, W. Yi, C. Yang, J. Guo, Y. Shi, S. Zhang, Z. Wang, C. Zhang, S. Jiang, A. Li, K. Yang, Q. Wu, G. Zhang, L. Sun, and Z. Zhao, “Superconductivity emerging from a suppressed large magnetoresistant state in tungsten ditelluride,” *Nature Communications* **6**, 7804 (2015).
- [8] X.-C. Pan, X. Chen, H. Liu, Y. Feng, Z. Wei, Y. Zhou, Z. Chi, L. Pi, F. Yen, F. Song, X. Wan, Z. Yang, B. Wang, G. Wang, and Y. Zhang, “Pressure-driven dome-shaped superconductivity and electronic structural evolution in tungsten ditelluride,” *Nature Communications* **6**, 7805 (2015).
- [9] A. A. Burkov and L. Balents, “Weyl semimetal in a topological insulator multilayer,” *Phys. Rev. Lett.* **107**, 127205 (2011).
- [10] A. A. Zyuzin, S. Wu, and A. A. Burkov, “Weyl semimetal with broken time reversal and inversion symmetries,” *Phys. Rev. B* **85**, 165110 (2012).
- [11] A. A. Zyuzin and A. A. Burkov, “Topological response in weyl semimetals and the chiral anomaly,” *Phys. Rev. B* **86**, 115133 (2012).
- [12] A. G. Grushin, “Consequences of a condensed matter realization of lorentz-violating qed in weyl semi-metals,” *Phys. Rev. D* **86**, 045001 (2012).
- [13] P. Hosur, X. Dai, Z. Fang, and X.-L. Qi, “Time-reversal-invariant topological superconductivity in doped weyl semimetals,” *Phys. Rev. B* **90**, 045130 (2014).
- [14] B. Yan and C. Felser, “Topological materials: Weyl semimetals,” *Annual Review of Condensed Matter Physics* **8**, 337 (2017).
- [15] A. Burkov, “Weyl metals,” *Annual Review of Condensed Matter Physics* **9**, 359 (2018).
- [16] S. Kobayashi and M. Sato, “Topological superconductivity in dirac semimetals,” *Phys. Rev. Lett.* **115**, 187001 (2015).
- [17] Z. Yan, Z. Wu, and W. Huang, “Vortex end majorana zero modes in superconducting dirac and weyl semimetals,” *Phys. Rev. Lett.* **124**, 257001 (2020).
- [18] G. Shipunov, I. Kovalchuk, B. R. Piening, V. Labracherie, A. Veyrat, D. Wolf, A. Lubk, S. Subakti, R. Giraud, J. Dufouleur, S. Shokri, F. Caglieris, C. Hess, D. V. Efremov, B. Büchner, and S. Aswartham, “Polymorphic ptbi_2 : Growth, structure, and superconducting properties,” *Phys. Rev. Materials* **4**, 124202 (2020).
- [19] V. Berezinskii, “Destruction of long-range order in one-dimensional and two-dimensional systems having a continuous symmetry group i. classical systems,” *Sov. Phys. JETP* **32**, 493 (1971).
- [20] J. M. Kosterlitz and D. J. Thouless, “Ordering, metastability and phase transitions in two-dimensional systems,” *Journal of Physics C: Solid State Physics* **6**, 1181 (1973).
- [21] D. E. Kharzeev, “The chiral magnetic effect and anomaly-induced transport,” *Progress in Particle and Nuclear Physics* **75**, 133 (2014).
- [22] A. A. Burkov, “Chiral anomaly and transport in weyl metals,” *Journal of Physics: Condensed Matter* **27**, 113201 (2015).
- [23] N. P. Armitage, E. J. Mele, and A. Vishwanath, “Weyl and dirac semimetals in three-dimensional solids,” *Rev. Mod. Phys.* **90**, 015001 (2018).
- [24] E. Witten, “Dyons of charge $e\theta/2\pi$,” *Physics Letters B* **86**, 283 (1979).
- [25] F. S. Nogueira, Z. Nussinov, and J. van den Brink, “Josephson currents induced by the witten effect,” *Phys. Rev. Lett.* **117**, 167002 (2016).
- [26] F. S. Nogueira, Z. Nussinov, and J. van den Brink, “Fractional angular momentum at topological insulator interfaces,” *Phys. Rev. Lett.* **121**, 227001 (2018).
- [27] F. S. Nogueira and J. van den Brink, “Absence of induced magnetic monopoles in maxwellian magnetoelectrics,” *Phys. Rev. Res.* **4**, 013074 (2022).
- [28] H. Kleinert, *Gauge Fields in Condensed Matter: Vol. 1: Superflow and Vortex Lines (Disorder Fields, Phase Transitions) Vol. 2: Stresses and Defects (Differential Geometry, Crystal Melting)* (World Scientific, 1989).
- [29] W. A. Little and R. D. Parks, “Observation of quantum periodicity in the transition temperature of a superconducting cylinder,” *Phys. Rev. Lett.* **9**, 9 (1962).
- [30] E. Babaev and M. Speight, “Semi-meissner state and neither type-i nor type-ii superconductivity in multicomponent superconductors,” *Phys. Rev. B* **72**, 180502 (2005).
- [31] V. Moshchalkov, M. Menghini, T. Nishio, Q. H. Chen, A. V. Silhanek, V. H. Dao, L. F. Chibotaru, N. D. Zhigadlo, and J. Karpinski, “Type-1.5 superconductivity,” *Phys. Rev. Lett.* **102**, 117001 (2009).
- [32] V. Shyta, J. van den Brink, and F. Nogueira, “to be published,”.
- [33] M. Stålhammar, D. Rudneva, T. H. Hansson, and F. Wilczek, “Emergent chern-simons interactions in 3+1 dimensions,” (2023), [arXiv:2309.10025 \[cond-mat.mes-hall\]](https://arxiv.org/abs/2309.10025).

Supplemental Material: vortex solution in a slab geometry

The vortex solution for a slab defined in the region $|z| < L/2$ is more easily obtained by considering the differential equations for the vector potential. The London equation for the vector potential reads,

$$-\nabla^2 \mathbf{A} + M^2 \mathbf{A} = \frac{M^2 \Phi_0}{2\pi} \frac{\hat{\varphi}}{r} - a \nabla \times \mathbf{A}. \quad (14)$$

Based on the infinite vortex solution, we consider the Ansatz,

$$A_r(r, z) = a \frac{M^2 \Phi_0}{2\pi} \int dp \frac{J_1(pr)}{(p^2 + M^2)^2 - a^2 p^2} \frac{\partial \beta(p, z)}{\partial z}, \quad (15)$$

$$A_\varphi(r, z) = \frac{M^2 \Phi_0}{2\pi} \int dp \frac{J_1(pr)(p^2 + M^2)}{(p^2 + M^2)^2 - a^2 p^2} \beta(p, z), \quad (16)$$

$$A_z(r, z) = -a \frac{M^2 \Phi_0}{2\pi} \int dp \frac{p J_0(pr)}{(p^2 + M^2)^2 - a^2 p^2} \beta(p, z), \quad (17)$$

$$B_r = -\frac{M^2 \Phi_0}{2\pi} \int dp \frac{(p^2 + M^2) J_1(pr)}{(p^2 + M^2)^2 - a^2 p^2} \frac{\partial \beta(p, z)}{\partial z}, \quad (18)$$

$$B_\varphi = -\frac{a M^2 \Phi_0}{2\pi} \int dp \frac{J_1(pr) \left[p^2 \beta - \frac{\partial^2 \beta(p, z)}{\partial z^2} \right]}{(p^2 + M^2)^2 - a^2 p^2}, \quad (19)$$

$$B_z = \frac{M^2 \Phi_0}{2\pi} \int dp \frac{p (p^2 + M^2) J_0(pr)}{(p^2 + M^2)^2 - a^2 p^2} \beta(p, z), \quad (20)$$

where the function $\beta(p, z)$ is determined by application of the boundary conditions, which imposes the continuity of \mathbf{A} and its derivatives with respect to z at the interfaces $z = \pm L/2$. With this we obtain,

$$\beta(p, z) = \begin{cases} e^{p(\frac{L}{2}-z)} \frac{[\tau_1 \sinh(\frac{L\tau_1}{2}) \cos(\frac{L\tau_2}{2}) - \tau_2 \cosh(\frac{L\tau_1}{2}) \sin(\frac{L\tau_2}{2})]}{p \cosh(\frac{L\tau_1}{2}) \cos(\frac{L\tau_2}{2}) + \tau_1 \sinh(\frac{L\tau_1}{2}) \cos(\frac{L\tau_2}{2}) - \tau_2 \cosh(\frac{L\tau_1}{2}) \sin(\frac{L\tau_2}{2})} \\ 1 - \frac{p \cosh(\frac{L\tau_1}{2}) \cos(\frac{L\tau_2}{2}) + \tau_1 \sinh(\frac{L\tau_1}{2}) \cos(\frac{L\tau_2}{2}) - \tau_2 \cosh(\frac{L\tau_1}{2}) \sin(\frac{L\tau_2}{2})}{p \cosh(\tau_1 z) \cos(\tau_2 z)} \\ e^{p(\frac{L}{2}+z)} \frac{[\tau_1 \sinh(\frac{L\tau_1}{2}) \cos(\frac{L\tau_2}{2}) - \tau_2 \cosh(\frac{L\tau_1}{2}) \sin(\frac{L\tau_2}{2})]}{p \cosh(\frac{L\tau_1}{2}) \cos(\frac{L\tau_2}{2}) + \tau_1 \sinh(\frac{L\tau_1}{2}) \cos(\frac{L\tau_2}{2}) - \tau_2 \cosh(\frac{L\tau_1}{2}) \sin(\frac{L\tau_2}{2})}, \end{cases} \quad (21)$$

where we defined,

$$\tau_1^2(p) = \frac{1}{2} \left(\sqrt{(p^2 + M^2)^2 - a^2 p^2} + p^2 + M^2 - \frac{a^2}{2} \right), \quad (22)$$

$$\tau_2^2(p) = \frac{1}{2} \left(\sqrt{(p^2 + M^2)^2 - a^2 p^2} - \left(p^2 + M^2 - \frac{a^2}{2} \right) \right). \quad (23)$$

We note that,

$$\tau_1(0) = \sqrt{4M^2 - a^2}/2, \quad \tau_2(0) = ia/2, \quad (24)$$

and thus we obtain the complex mass scales $M_\pm = \tau_1(0) \pm \tau_2(0)$ that appear in the infinite vortex solution in the main text.

Up to linear order in a ,

$$B_\varphi = -\frac{a M^2 \Phi_0}{2\pi} \int dp \frac{J_1(pr) \left[p^2 \beta_0(p, z) - \frac{\partial^2 \beta_0(p, z)}{\partial z^2} \right]}{(p^2 + M^2)^2} \quad (25)$$

$$B_r = -\frac{M^2 \Phi_0}{2\pi} \int dp \frac{J_1(pr)}{(p^2 + M^2)} \frac{\partial \beta_0(p, z)}{\partial z} \quad (26)$$

$$B_z = \frac{M^2 \Phi_0}{2\pi} \int dp \frac{p J_0(pr)}{(p^2 + M^2)} \beta_0(p, z), \quad (27)$$

where the notation $\beta_0(p, z)$ refers to the function $\beta(p, z)$ with $a = 0$,

$$\beta_0(p, z) = \begin{cases} \frac{\tau e^{p(\frac{L}{2}-z)}}{\tau + p \coth(\frac{\tau L}{2})}, & z > \frac{L}{2} \\ 1 - \frac{p \cosh(\tau z)}{p \cosh(\frac{\tau L}{2}) + \tau \sinh(\frac{\tau L}{2})}, & -\frac{L}{2} < z < \frac{L}{2} \\ \frac{\tau e^{p(\frac{L}{2}+z)}}{\tau + p \coth(\frac{\tau L}{2})}, & z < -\frac{L}{2}, \end{cases} \quad (28)$$

$$\tau = \sqrt{p^2 + M^2}.$$
